analytical chemistry

Article

Cite This: Anal. Chem. 2018, 90, 3205−3210

pubs.acs.org/ac

A New Concentration Jump Strategy Reveals the Lifetime of i-Motif at Physiological pH without Force

Sagun Jonchhe, Prakash Shrestha, Katia Ascencio, and Hanbin Mao*

Department of Chemistry and Biochemistry, Kent State University, Kent, Ohio 44242, United States

Supporting Information

ABSTRACT: Concentration jumps for kinetics measurement remain a challenge for single-molecule techniques, which have demonstrated superior signal-to-noise levels compared to ensemble average approaches. Currently, all concentration jumps use mixing strategies. Here, we report a simple and drastically different jump strategy by rapid transportation of molecules between two side-by-side laminar streams in 80 ms. This allowed us to measure the lifetime of bioactive DNA i-motif structures at physiological pH without force. We placed a human telomeric i-motif inside a DNA hairpin-based mechanical reporter. Since the folded or unfolded state of the hairpin correlates with that of the i-motif, by recording hairpin transitions, a half-life of ∼3 s was found for the DNA i-motif at neutral pH without force. Such a lifetime is sufficient for i-motif to interact with proteins to modulate cellular processes. We anticipate this concentration jump offers a generic platform to investigate single-molecule kinetics.

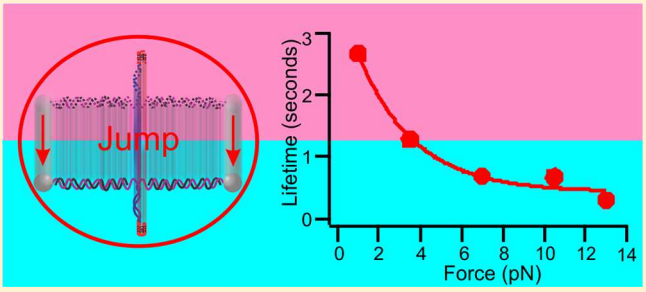

To measure rapid kinetics of chemical or biochemical reactions in different chemical environments, it is essential to synchronize reaction processes by use of concentration jumps. Almost all concentration jumps use rapid mixing of different chemicals. The mixing time can be controlled within milliseconds in the widely used stopped-flow methods,[1−3] which use spectroscopic detection methods such as absorbance and fluorescence.[4] However, ultrasensitive detection has yet to be achieved at the single-molecule level in stopped-flow methods. Only scattered single-molecule investigations have been carried out in which microfluidic mixing is used for the concentration jump.[5−7] With this approach, different molecules are sampled transiently in free solution. To monitor the entire reaction pathway, single molecules should be immobilized on a surface.

Synchronization is not always necessary for single-molecule reactions carried out at the condition where both reactants and products populate. Under such circumstances, transition kinetics of the reaction can be estimated from the dwell time of each species that can interconvert to each other.[8] To accurately record the dwell time of individual molecules, each molecule should be tracked for sufficient time. In single-molecule fluorescence approaches, surface immobilization of the molecule provides a means for the tracking.

In force-based single-molecular investigations in which optical tweezers or atomic force microscopic (AFM) instruments are used, individual molecules can be tethered between two surfaces for the purpose of tracking.[9−11] In the chemical environment that does not allow the interconversion between two species, rapid change of the environment via concentration jump becomes necessary for immobilized single molecules. However, both fluorescence-based and force-based single-molecule approaches have compatibility issues in concentration jumps that use mixing as a mechanism. For example, fluorescence molecules damaged by processes such as photobleaching should be frequently replaced on the surface of the observation chamber in a mixing device. In single-molecule force spectroscopy, the rapid variation in flow rates during mixing is detrimental to force measurements by AFM or optical tweezers.

Herein, we innovated a simple concentration jump approach with a transportation-based mechanism, which is drastically different from mixing-based methods. Using two side-by-side laminar flows inside microfluidic channels, we were able to move individual molecules between different chemical environments within 80 ms. With this microfluidic single-molecule concentration jumping, we measured the lifetime of human telomeric DNA i-motif, a structure that is sensitive to hydronium concentrations, in a pH range of 6.0−7.0. Previously, the lifetime of i-motif has only been measured inside a nanopore cavity at a mechanical force roughly estimated.[12] To reliably record nanometer-sized signals of i-motif folding and unfolding transitions, we placed the i-motif inside the loop of a hairpin mechanophore. Under a specific force, the mechanophore carries out the transition between folded and unfolded hairpins (or mechanoescence).[11,13] Since this transition is controlled by whether the i-motif is folded or not in the hairpin loop, it allows us to retrieve the i-motif lifetime in the force range that falls into that of the stall force of

Received: November 11, 2017
Accepted: February 5, 2018
Published: February 5, 2018

DOI: 10.1021/acs.analchem.7b04661
Anal. Chem. 2018, 90, 3205−3210

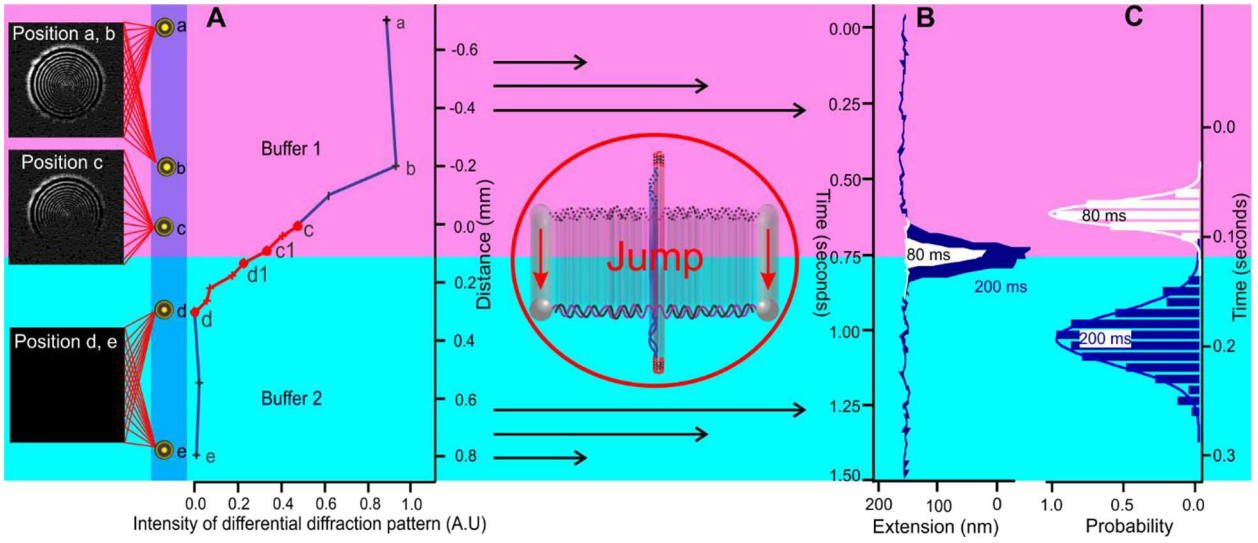

Figure 1. Transportation-based concentration jump method. (A) Quantification of the diffraction pattern of a laser beam focused at different locations (marked a–e) across two laminar streams. Selected images for differential diffraction patterns are shown to the left. The interfacial regions (c–d) are highlighted in red. (B) Change in the extension of a single-molecule construct tethered between the two optically trapped beads (gray spheres in the red circular inset; see Figure S5 for details) during the rapid movement from position c to d. The movement leads to different Stokes force experienced by the two optically trapped beads with different sizes, which causes a perturbation in the bead-to-bead distance (extension). White and blue traces depict the jumps across the 50 μm (c1 → d1) and 300 μm (c → d) distances, respectively. (C) Durations of the perturbation, which correlate with the jump time, plotted in histograms for the jumps across the 300 μm (c→ d, blue) and 50 μm (c1 → d1, white) distances, respectively. Solid curves depict Gaussian fittings.

DNA or RNA polymerases (~14 pN).[14,15] At neutrality without force, we found DNA telomeric i-motif has a half-life of ~3 s, which provides a support for the biological functions of i-motif inside cells.[16] We anticipate our innovative approaches are generic to evaluate the transition kinetics of biological structures in unfavorable environments not accessible to ensemble average methods.

EXPERIMENTAL SECTION

Materials and Reagents. DNA oligomers were obtained from Integrated DNA Technology (IDT, Coralville, IA), further purified by polyacrylamide gel electrophoresis (PAGE), and stored at −20 °C. Polystyrene beads coated with streptavidin or digoxigenin antibody were obtained from Spherotech (Lake Forest, IL). High-performance motorized actuator (VP- 25AA) was purchased from Newport Corp. (Irvine, CA). Unless specified otherwise, all chemicals were purchased from VWR (Radnor, PA) with a minimum purity of >99.0%.

Preparation of DNA Constructs. DNA construct was synthesized by three-piece ligation of the P1, P2, and C23 fragments as shown in Figure S1.[13,17] The 2028-bp handle was prepared by polymerase chain reaction (PCR) amplification of the pBR322 template (New England Biolabs, NEB) with a 5′-biotinylated primer, 5′-GCA TTA GGA AGC CCA GTA GTA GG-3′ (IDT, Coralville, IA). The PCR product was purified by agarose gel and digested by *Xba*I restriction enzyme (NEB). For preparation of the 2690-bp handle, pEGFP plasmid (Clontech, Mountain View, CA) was digested by *Sac*I (NEB) and *Eag*I (NEB), followed by purification and the labeling with digoxigenin (Dig) by use of 18 μM Dig-dUTP (Roche, Indianapolis, IN) and terminal transferase (Fermentas, Glen Burnie, MD) at the 3′-end. To prepare the P1 fragment (Figure S1), B1 and B5 were annealed first, followed by ligation with the 2028-bp handle by use of T4 DNA ligase (NEB). For preparation of the P2 fragment, B3 and B4 were annealed first, followed by ligation with the 2690-bp handle by use of T4 DNA ligase. Fragments P1, P2, and C23 were then mixed, heated to 90 °C, and rapidly cooled on ice to facilitate hairpin formation. Finally, the three pieces were ligated by use of T4 DNA ligase, resulting in the final construct.

Design of Microfluidic Chamber. A four-channel microfluidic chamber was made by sandwiching a parafilm (thickness 0.127 mm, Bemis Co., Neenah, WI) between two pieces of cover glass (#1, VWR, size 24 × 60 mm) using thermal bonding (90 °C) with a weight (~5 lb) for 20 s. The parafilm contained a desired pattern (see Figure S3) cut by a laser (Versa Laser, Scottsdale, AZ). The microfluidic chamber contains four channels with a width of 1.6 mm each. The top and bottom channels are used to introduce streptavidin- and Dig-antibody-coated polystyrene beads, respectively. Two middle channels merge from the midway to form a Y-shaped flow pattern. The two middle channels were connected to the top and bottom channels with micropipettes (Garner Glass Co., i.d. 25 μm). Inlet (left) and outlet (right) holes through one of the cover glasses were drilled by the Versa laser cutter described above. The chamber was fixed in a homemade bracket, which was controlled by a Newport stage equipped with an actuator (high-performance motorized actuator, VP-25AA; Newport, Irvine, CA) for concentration jump experiments (see Figure S3). Two buffers with different chemical compositions were separately introduced to the two middle channels by a Harvard Apparatus pump (Harvard Apparatus, South Natick, MA) with a flow rate maintained at 0.6 μL/min (or 0.077 mm/s).

Laser Tweezers Instrumentation. Detailed description of the laser tweezers has been reported previously.[18] In short, a diode-pumped solid-state laser (1064 nm, 5 W, IPG Photonics) was used to generate S- and P-polarized laser light for separate trapping of two polystyrene beads. A steerable mirror (Nano-

DOI: 10.1021/acs.analchem.7b04661
Anal. Chem. 2018, 90, 3205−3210

MTA, Mad City Laboratories, Madison, WI) at a conjugate plane of the back focal plane of a focusing objective [Nikon CFI-PlanApochromat 60×, numerical aperture (NA) 1.2, water immersion, working distance ∼320 μm] was used to control the S-polarized light. The position of the laser point was detected by two position-sensitive photodetectors (PSD, DL100, Pacific Silicon Sensor). The power of each trap was fixed at 350 mW.

Mechanical Unfolding and Concentration Jump Experiments. In the stabilized flow inside the microfluidic chamber, two traps were employed to capture two different beads at 25 °C as described above (Figure S5). The trap positions were aligned parallel to the flow. By the steerable mirror, one of the traps, which contains the bead immobilized with the DNA construct through the Dig−anti-Dig interaction (see section SVII in Supporting Information), was moved close to the streptavidin-coated bead trapped by the other laser. By the streptavidin−biotin interaction, the single-molecule DNA construct was tethered between the two trapped beads. Once a tether was obtained (Figure S5), force ramping at 5.5 pN/s loading rate was carried out to mechanically unfold DNA hairpin and/or i-motif under different buffer conditions. The force was recorded in a Labview 8 (National Instruments, Austin, TX) program and treated by Igor programs (Wavemetrics, Portland, OR) to generate force−extension curves. For concentration jump experiments, the tether containing the i-motif@hairpin construct was maintained at a constant force of ∼14 pN in the pH 5.5 buffer channel. At this force, rapid folding and unfolding transition of the DNA hairpin (mechanoescence)[13] was observed, indicating i-motif was folded in the loop of the hairpin. The mechanoescence continued until i-motif was unfolded in the DNA hairpin loop, which was immediately followed by increase of the extension, indicating the unfolding of the hairpin itself. The construct at the fixed force was slowly moved to the start position of the concentration jump close to the interface. The destiny of the concentration jump was determined at the position beyond which differential diffraction pattern stays the same (point d in Figure 1A). The jump was accomplished by rapid chamber movement controlled by a high-performance motorized actuator (VP-25AA, Newport, Irvine, CA). The extension data for the DNA construct during the entire process were continuously recorded by a Labview 8 program at 1 kHz bandwidth. The lifetime of the i-motif was estimated from the end of the concentration jump to the end of the mechanoescence (see Figure 3A).

RESULTS AND DISCUSSION

Transportation-Based Single-Molecule Concentration Jump in Microfluidics. Rapid transportation of individual molecules was achieved between two microfluidic streams flowed side-by-side (Figure 1 and Figure S3). Due to the laminar flow inside the microfluidic channel of 3.9 × 0.12 mm in cross section (Reynolds number Re = 0.02; see Figure S3 and eq S2 in Supporting Information for calculation),[19] chemicals contained in each stream do not exchange via rapid convectional mixing. Instead, diffusional mixing occurs between the two streams through their interface (see eq S3 in Supporting Information for calculation). For effective concentration jumps, it is necessary to determine the concentration profile at the interface.

Fluorescent molecules can be used to estimate the concentration profile at the interface.[20] However, not every buffer component has fluorescence, while its concentration profile does not necessarily follow that of fluorescent molecules. We noticed that concentration jump requires the switch between two buffers with different physical properties such as viscosity, density, and/or ionic strength, which are often accompanied by variation in the refractive index. By monitoring of this refractive index change using a laser beam passing through different buffer streams, it is possible that the concentration profile of the interface can be determined.

To this end, we first injected two laminar streams of different buffers inside a microfluidic chamber (Figure 1A and Figure S3). To stabilize the flow at the interface, we placed the buffer with higher density (100 mM Tris +100 mM KCl) below that of lower density [10 mM 2-(*N*-morpholino)ethanesulfonic acid (MES) + 100 mM KCl]. The stable interface was confirmed by trajectories of 1.86 μm polystyrene beads released from optical traps. The concentration jump was kept 0.6 mm downstream of the partitioning membrane to ensure minimal surface effect (Figure S3). Along the vertical jumping path across this location, hydronium diffusion from the neighboring stream displayed a penetration depth of 125 μm at the experimental flow rate (eq S3 in Supporting Information). Therefore, the pH at the jump destination (∼150 μm below the interface, see location d discussed below) should not be affected by the diffusional mixing of hydroniums from the top buffer stream.

By adjusting the focus of one of the 1064 nm laser beams passing through the laminar streams, diffraction (Airy)[21] rings were observed at different locations (a−e) along the vertical transportation path (Figure S4). Intensity of the Airy rings at each location was compared to that of point d (Figure 1A). We found that d is the location in the bottom stream closest to the interface that has the same pattern as location e. Since e represents the bulk of the bottom stream, this suggests that d has the same buffer properties, such as chemical concentrations, as the bottom buffer. Therefore, location d was chosen as the end point of the concentration jump.

Next, we used a single-molecule DNA tethered between two optically trapped beads as a sensor to measure the transportation time from the start points in the top stream to location d (Figure 1 and Figure S5; see Figure S1 for construct preparation). A constant force of ∼14 pN was maintained in the tethered molecule during the transportation. When the chamber was rapidly moved (or jumped) by a motor along the transportation path, the tension inside the molecule changed. To maintain the same ∼14 pN force, the extension of the molecule was varied by adjusting one of the optically trapped beads with a steerable mirror (see Experimental Section). Such a variation was indicative of the jump time (Figure 1B,C). While position b is the closest point to the interface that remains the same chemical concentration as the bulk of the upper stream, it has a relatively long distance to point d (500 μm; jump time 300 ms). With the transportation distance decreased to 50 μm (c1→ d1 in Figure 1A), the jump time is reduced to 80 ms (Figure 1B,C). However, the closeness of c1 or d1 to the interface makes them vulnerable to flow fluctuations. Since location c in the upper stream is significantly away from the interface, this position was chosen as the starting point for the jumps. The finalized path (c → d 300 μm) showed 200 ms average jump time (Figure 1C). It is noteworthy that, with optimization of trap stiffness, properties of trapped particles (size and refractive index), and flow rate, the jump time can be reduced further.

A DNA Hairpin Mechanophore Reports Folded and Unfolded States of Human Telomeric i-Motif. As a proof

DOI: 10.1021/acs.analchem.7b04661
Anal. Chem. 2018, 90, 3205−3210

of principle, we used this new concentration jump platform to probe the lifetime of telomeric DNA i-motif (5′-CCC TAA CCC TAA CCC TAA CCC) at different pH and force. Discovered in the 1990s,[22] DNA i-motif has demonstrated regulatory functions for oncogene transcriptions inside cells recently.[16] As a DNA secondary structure, i-motif consists of intercalated stacks of hemiprotonated cytosine (C)-cytosine (or C-CH$^+$) pairs, which renders i-motif pH-sensitive.[22] While hemiprotonation occurs readily at pH 5.5, deprotonation of cytosine at neutral pH can dissolve the i-motif structure rapidly.[12,23] The rather low formation probability of i-motif at neutrality made it highly challenging to accurately measure the lifetime of i-motif by use of ensemble average approaches. Formation of i-motif can be investigated by various single-molecule approaches.[12,24] Mechanical unfolding of individual telomeric i-motifs is expected to cause an elongation signal of ~8.3 nm (see Supporting Information for calculation). Such a small signal can be easily overlooked in experiments, especially when the i-motif is unfolded during transportation or when the background noise is high at low tensions (<5 pN). To address this issue, we used a DNA hairpin as a mechanophore to report the folding states of i-motif in real time.

Recent investigations on individual DNA hairpins have revealed that, at ~14 pN, DNA hairpin undergoes rapid folding and unfolding processes.[11] This so-called mechanoescence[13] slows down significantly with increasing loop size of the hairpin. Using this property, we placed the telomeric i-motif-forming sequence (see above) inside a hairpin loop (see Experimental Section and Figure S1 for construct preparation). The mechanical properties of the i-motif@hairpin construct were quantified in force–extension curves[24] (Figure 2; see Experimental Section). At pH 5.5, the unfolding force for the hairpin (16.6 pN) was lower than that of the i-motif (30.8 pN) (Figure 2A), indicating that the hairpin should be unfolded before the i-motif. At pH 7.4, the i-motif did not form and the unfolding force for the hairpin was 15.4 pN (Figure 2B). Based on these results, a pH–force phase diagram was constructed (Figure 2C). In the acidic environment when the force in the DNA tether is low, the i-motif and DNA hairpin remain folded (state I in Figure 2C). With force increased above 16.6 pN but below the unfolding force of the i-motif (30.8 pN), the hairpin unfolds while the i-motif remains folded (state II). In the less acidic environment (i.e., close to pH 7), when the tension in the DNA tether is below 15 pN, the i-motif is unfolded whereas hairpin remains folded (state III). Further increase in the tension (>15.4 pN) at the same pH would unfold both the hairpin structure and i-motif (state IV).

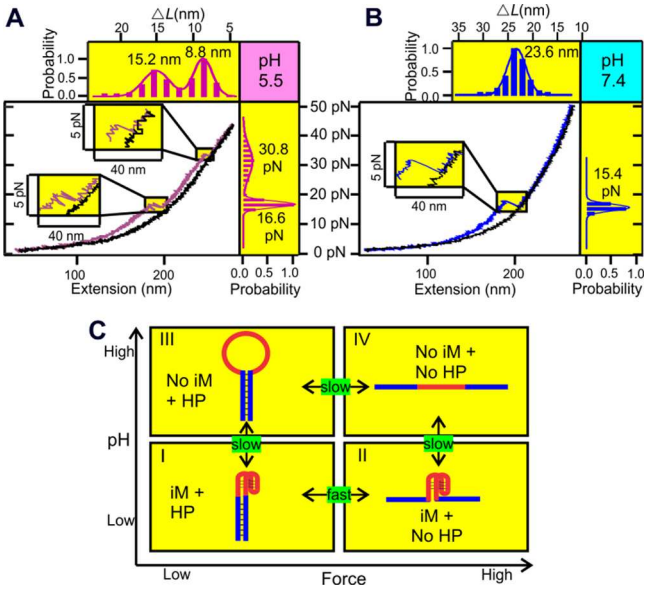

Figure 2. (A, B) Force–pH behavior of i-motif@hairpin construct: force versus extension plots at (A) pH 5.5 and (B) pH 7.4. (Insets) Expanded views of unfolding features. Colored and black traces depict stretching and relaxing processes, respectively. ΔL and force histograms are shown at the top and to the right, respectively. (C) pH–force phase diagram of the construct. State I, both i-motif (iM, red) and hairpin (HP, blue) are folded; state II, i-motif is folded whereas hairpin is unfolded; state III, i-motif is unfolded whereas hairpin is folded; state IV, both i-motif and hairpin are unfolded.

Compared to the unfolded i-motif in the hairpin loop, the size of the loop is much smaller when the i-motif is folded (end-to-end distances are ~0.7 nm[24] and 8.3 nm for the folded and unfolded telomeric i-motifs, respectively; see Figure S2). Such a variation indeed caused different folding/unfolding transitions (mechanoescence) of the DNA hairpin: while folded i-motif led to rapid mechanoescence of the hairpin (states I and II in Figures 2C and 3A), unfolded i-motif caused fewer hopping events (states III and IV). Since increased loop size reduces the mechanical stability of the hairpin,[11] as soon as the i-motif was unfolded in the loop, the hairpin itself unfolded (state IV).

Kinetics of Individual Telomeric i-Motif Structures at Physiologically Relevant pH and Force Ranges. To measure the transition kinetics of the telomeric i-motif, we first let i-motif fold in the top laminar buffer stream at pH 5.5 (see Figure 1). The mechanoescence of the hairpin was observed at a constant force of ~14 pN (Figure 3A). In the bottom stream, we injected the buffer with higher density at pH

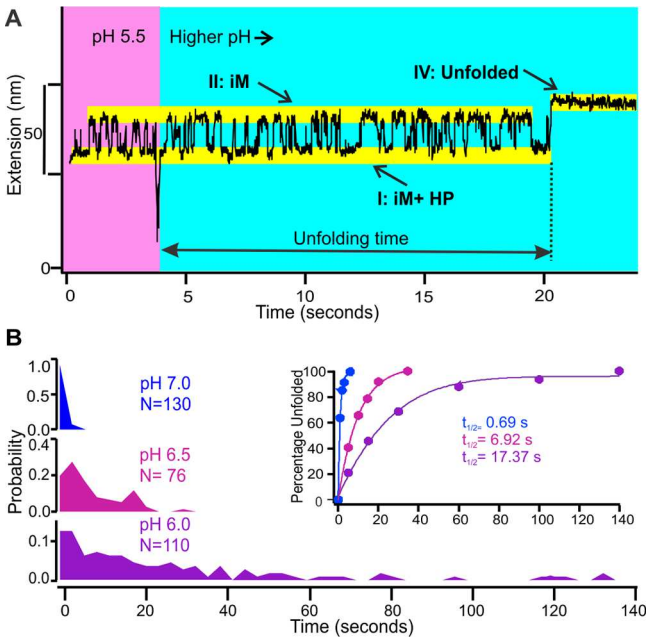

Figure 3. Lifetime of telomeric i-motif at 7 pN experienced force. (A) Extension versus time plot before (pH 5.5) and after (higher pH) transportation of the i-motif. Refer to Figure 2C for different states (I, II, and IV). (B) Histogram of unfolding time for telomeric i-motif at pH 6.0, 6.5, or 7.0. (Inset) Unfolding percentage of i-motif vs cumulative time. Plots are fitted with single-exponential curves.

DOI: 10.1021/acs.analchem.7b04661
Anal. Chem. 2018, 90, 3205–3210

5.5−7.4 (see Figure 1). During and after the transportation c → d (Figure 1A), the same force was kept to maintain the mechanoescence of the DNA hairpin while the i-motif remained folded in the loop. When i-motif was unfolded, the mechanoescence immediately ceased. At the same time, the molecular extension became longer as the nucleotides in the folded i-motif were released to give fully stretched construct (state IV in Figure 3A).

The unfolding time of the i-motif was measured from the end of transportation to the fully unfolded state of the DNA construct at pH 6.0, 6.5, or 7.0 (Figure 3A). At each pH, we measured unfolding time from ~100 jumping events (Figure 3B), which was further analyzed as the percentage of unfolded i-motif versus accumulated unfolding time (see Supporting Information). We found that, with increasing pH, the unfolding time (or lifetime) decreases. In fact, the unfolding time of i-motif at pH 7.4 could not be determined, as unfolding occurred during transportation (<200 ms).

Single-exponential fitting of the unfolding percentage traces (Figure 3B, inset) revealed half-lives ($t_{1/2}$; see eq S6 in Supporting Information) of 17.37, 6.92, and 0.69 s for i-motif at pH 6.0, 6.5, and 7.0, respectively, at the average experienced force of 7 pN. As a control, the $t_{1/2}$ at pH 5.5 was found to be 46.23 s (Figure S6). When the hairpin is folded, i-motif does not experience any force. However, when hairpin is unfolded, the tension (14 pN) in the construct directly applies to i-motif. Given that the folded and unfolded hairpin populations remained equal before the telomeric i-motif was unfolded, the folded i-motif experienced an average force of 7 pN (see Supporting Information for detailed calculation). The pH effect on the lifetime of i-motif can be well explained by the availability of protons. The higher the pH, the fewer the protons and the shorter the lifetime, as hemiprotonated C-CH$^+$ pairs are more difficult to maintain in i-motif structures.[12,22] To evaluate the effect of buffer density on the lifetime of telomeric i-motif, we repeated the jump experiments in the two buffers with the same density (10 mM MES + 100 mM KCl for the top stream at pH 5.5 and 16.5 mM Tris +100 mM KCl for the bottom stream at pH 7.0). Since we obtained identical half-lives (0.69 ± 0.28 s at 7 pN; see Figure S7) for the telomeric i-motif unfolding, it demonstrates that these buffer densities had a negligible effect on the unfolding kinetics of the i-motif structure.

To explore the effect of the average experienced force on unfolding kinetics of the i-motif at pH 7, tensions in the DNA construct were fine-turned around 14 pN to populate different ratios of folded versus unfolded hairpins during and after each concentration jump. On the basis of these population ratios (eq S7 in Supporting Information), average forces experienced by the i-motif were separated into five groups (1.0, 3.5, 7.0, 10.5, and 13.0 pN; Figure 4A). The $t_{1/2}$ showed a decreasing order with increasing force (2.66, 1.28, 0.69, 0.67, and 0.30 s, respectively; see Figure 4A, insets). We extrapolated the unfolding kinetics (k_{unfold}) of i-motif to zero experienced force using an exponential function (the Bell model;[25] see eq S9 in Supporting Information). The linear relationship shown in Figure 4B suggests that average experienced force is a reasonable approximation for the external force described by the Bell model. At neutrality, the $t_{1/2}$ of the i-motif (2.60 s at 0 pN; see Figure 4B) is much shorter than the time required in regular mechanical unfolding experiments. By this new technique, we can apply mechanical forces to the i-motif structures and investigate the effect of the physiologically

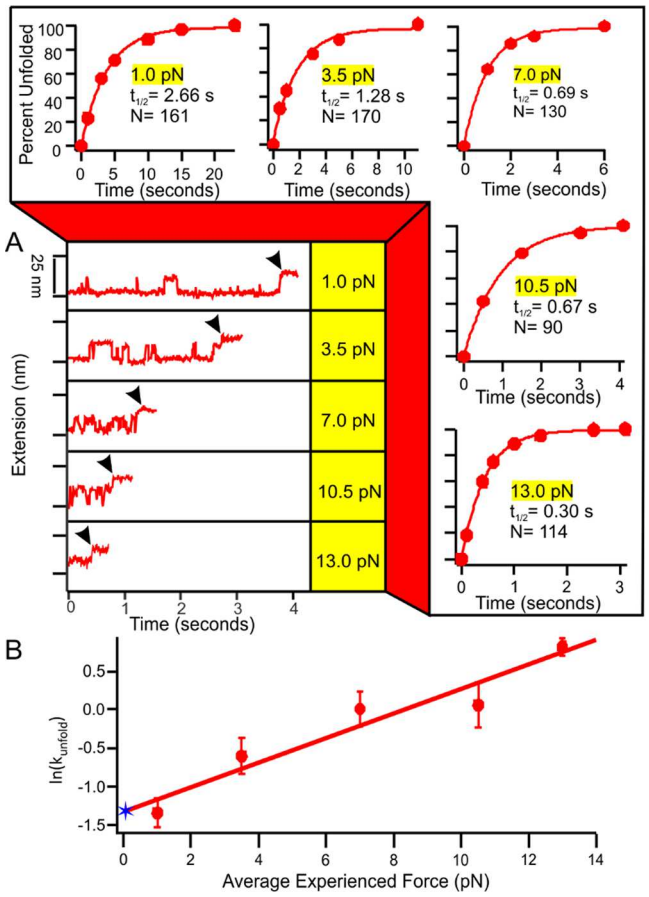

Figure 4. Force effect on the unfolding of telomeric i-motif at pH 7. (A) Effect of average experienced force on i-motif half-life ($t_{1/2}$). Time 0 depicts the end of transportation, and arrowheads indicate unfolded i-motif and hairpin (state IV in Figure 3A). Unfolded percentage vs time is plotted at an average experienced force of 0, 3.5, 7.0, 10.5, or 13.0 pN. Solid curves depict single-exponential fittings (see Supporting Information). (B) Extrapolation of unfolding rate constant (k_{unfold}) to 0 pN (blue star) with the Bell model (solid line) reveals $t_{1/2}$ = 2.60 s (see eq S6 in Supporting Information). Error bars depict the standard deviation from three sets of experiments.

relevant forces on the transition dynamics of secondary DNA structures.[14,15,26] This clearly testified to the uniqueness of the concentration jump to retrieve information inaccessible to other methods. Compared to nanopore-based lifetime measurement of i-motif,[12] our approach has increased throughput. Provided that only a minute population of i-motif forms close to the neutral pH,[24] the chance to observe folded i-motif is low if an experiment is performed at pH 7. In our method, each i-motif is readily folded at low pH and then transported to neutral pH for lifetime measurement with much increased efficiency. The i-motif lifetimes obtained from conventional stopped-flow assays ($t_{1/2}$ = 9.74 s at pH 7.02 without force)[27] and nanopore investigations ($t_{1/2}$ = 0.02 s at pH 6.8 under 10 pN force)[12] are comparable with ours. In fact, our results are located between the values obtained by these two methods, confirming the accuracy of our approach.

To the best of our knowledge, these jump experiments represent the first time the half-life of i-motif has been determined at physiological pH without external force at the single molecular level.[12] Inside cells, there are specific conditions that facilitate the formation of i-motif, which include negatively supercoiled DNA templates,[28,29] molecular crowded

DOI: 10.1021/acs.analchem.7b04661
Anal. Chem. 2018, 90, 3205−3210

environment,[30] C-rich sequence availability,[31] and nanoconfined cavities.[32] Once folded i-motifs encounter unfavorable conditions such as increased pH, the half-life of the structure decreases. Our finding that i-motif can survive for ∼3 s in physiological environment (0 pN and pH 7) provides a time window for the i-motif to interact with other cellular components, such as proteins, for potential biological activities.

CONCLUSIONS

In summary, a new method of single-molecule concentration jump was successfully demonstrated that uses the rapid transportation between two laminar streams in a microfluidic chamber. With this method, we revealed that telomeric i-motif has faster unfolding kinetics with increasing pH or force. At neutrality without force, the i-motif showed a $t_{1/2}$ of 2.60 s, which provides a sufficient window for the i-motif to partake in biological functions. We expect this concentration jump strategy is generic for single-molecule investigations in unfavorable chemical environments.

ASSOCIATED CONTENT

Supporting Information

The Supporting Information is available free of charge on the ACS Publications website at DOI: 10.1021/acs.analchem.7b04661.

Additional text and equations and seven figures describing synthesis of DNA constructs, calculation of change-in-contour-length (ΔL) and Reynolds number, determination of and diffusion across the interface between two laminar streams, preparation of microfluidic chambers and DNA samples, mechanical unfolding and concentration jump experiments, and unfolding of telomeric i-motif (PDF)

AUTHOR INFORMATION

Corresponding Author

* E-mail: hmao@kent.edu,Tel: +13306729380.

ORCID

Sagun Jonchhe: 0000-0003-4361-6641
Prakash Shrestha: 0000-0001-8752-4170
Hanbin Mao: 0000-0002-6720-9429

Author Contributions

The manuscript was written through contributions of all authors.

Notes

The authors declare no competing financial interest.

ACKNOWLEDGMENTS

We thank the NSF (CHE-1609514 and CHE-1415883 (partially)) for financial support.

REFERENCES

(1) Song, H.; Ismagilov, R. F. *J. Am. Chem. Soc.* **2003**, *125*, 14613−14619.
(2) Zijlstra, N.; Dingfelder, F.; Wunderlich, B.; Zosel, F.; Benke, S.; Nettels, D.; Schuler, B. *Angew. Chem., Int. Ed.* **2017**, *56*, 7126−7129.
(3) Krantz, B. A.; Sosnick, T. R. *Biochemistry* **2000**, *39*, 11696−11701.
(4) Qu, X.; Smith, G. J.; Lee, K. T.; Sosnick, T. R.; Pan, T.; Scherer, N. F. *Proc. Natl. Acad. Sci. U. S. A.* **2008**, *105*, 6602−6607.
(5) Gambin, Y.; VanDelinder, V.; Ferreon, A. C. M.; Lemke, E. A.; Groisman, A.; Deniz, A. A. *Nat. Methods* **2011**, *8*, 239−241.
(6) Wunderlich, B.; Nettels, D.; Benke, S.; Clark, J.; Weidner, S.; Hofmann, H.; Pfeil, S. H.; Schuler, B. *Nat. Protoc.* **2013**, *8*, 1459−1474.
(7) Pfeil, S. H.; Wickersham, C. E.; Hoffmann, A.; Lipman, E. A. *Rev. Sci. Instrum.* **2009**, *80*, 055105.
(8) Bayley, H.; Cremer, P. S. *Nature* **2001**, *413*, 226−230.
(9) Wuite, G. J. L.; Smith, S. B.; Young, M.; Keller, D.; Bustamante, C. *Nature* **2000**, *404*, 103−106.
(10) Rivetti, C.; Guthold, M.; Bustamante, C. *EMBO J.* **1999**, *18*, 4464−4475.
(11) Woodside, M. T.; Behnke-Parks, W. M.; Larizadeh, K.; Travers, K.; Herschlag, D.; Block, S. M. *Proc. Natl. Acad. Sci. U. S. A.* **2006**, *103*, 6190−6195.
(12) Ding, Y.; Fleming, A. M.; He, L.; Burrows, C. J. *J. Am. Chem. Soc.* **2015**, *137*, 9053−9060.
(13) Mandal, S.; Koirala, D.; Selvam, S.; Ghimire, C.; Mao, H. *Angew. Chem., Int. Ed.* **2015**, *54*, 7607−7611.
(14) Galburt, E. A.; Grill, S. W.; Wiedmann, A.; Lubkowska, L.; Choy, J.; Nogales, E.; Kashlev, M.; Bustamante, C. *Nature* **2007**, *446*, 820−823.
(15) Mejia, Y. X.; Mao, H.; Forde, N. R.; Bustamante, C. *J. Mol. Biol.* **2008**, *382*, 628−637.
(16) Kang, H.-J.; Kendrick, S.; Hecht, S. M.; Hurley, L. H. *J. Am. Chem. Soc.* **2014**, *136*, 4172−4185.
(17) Koirala, D.; Yu, Z.; Dhakal, S.; Mao, H. *J. Am. Chem. Soc.* **2011**, *133*, 9988−9991.
(18) Mao, H.; Luchette, P. *Sens. Actuators, B* **2008**, *129*, 764−771.
(19) Kenis, P. J. A.; Ismagilov, R. F.; Takayama, S.; Whitesides, G. M.; Li, S. L.; White, H. S. *Acc. Chem. Res.* **2000**, *33*, 841−847.
(20) Walker, D. A. *J. Phys. E: Sci. Instrum.* **1987**, *20*, 217.
(21) Hecht, E. *Optics*, 4th ed.; Pearson Education: Singapore, 2005.
(22) Gehring, K.; Leroy, J. L.; Guéron, M. *Nature* **1993**, *363*, 561−564.
(23) Nesterova, I. V.; Nesterov, E. E. *J. Am. Chem. Soc.* **2014**, *136*, 8843−8846.
(24) Dhakal, S.; Schonhoft, J. D.; Koirala, D.; Yu, Z.; Basu, S.; Mao, H. *J. Am. Chem. Soc.* **2010**, *132*, 8991−8997.
(25) Schlierf, M.; Rief, M. *Biophys. J.* **2006**, *90*, L33−L35.
(26) Yin, H.; Wang, M. D.; Svoboda, K.; Landick, R.; Block, S. M.; Gelles, J. *Science* **1995**, *270*, 1653−1657.
(27) Chen, C.; Li, M.; Xing, Y.; Li, Y.; Joedecke, C.-C.; Jin, J.; Yang, Z.; Liu, D. *Langmuir* **2012**, *28*, 17743−17748.
(28) Selvam, S.; Koirala, D.; Yu, Z.; Mao, H. *J. Am. Chem. Soc.* **2014**, *136*, 13967−13970.
(29) Selvam, S.; Mandal, S.; Mao, H. *Biochemistry* **2017**, *56*, 4616−4625.
(30) Rajendran, A.; Nakano, S.-i.; Sugimoto, N. *Chem. Commun.* **2010**, *46*, 1299−1301.
(31) Fleming, A. M.; Ding, Y.; Rogers, R. A.; Zhu, J.; Zhu, J.; Burton, A. D.; Carlisle, C. B.; Burrows, C. J. *J. Am. Chem. Soc.* **2017**, *139*, 4682−4689.
(32) Shrestha, P.; Jonchhe, S.; Emura, T.; Hidaka, K.; Endo, M.; Sugiyama, H.; Mao, H. *Nat. Nanotechnol.* **2017**, *12*, 582−588.

DOI: 10.1021/acs.analchem.7b04661
Anal. Chem. 2018, 90, 3205−3210